Journal of Materials Chemistry C

ROYAL SOCIETY OF CHEMISTRY

PAPER

View Article Online
View Journal | View Issue

Cite this: J. Mater. Chem. C, 2022, 10, 11775

Engineering the HOMO–LUMO gap of indeno[1,2-*b*]fluorene†‡

Raquel Casares, [a] Álvaro Martínez-Pinel, [a] Sandra Rodríguez-González, [b] Irene R. Márquez, [c] Luis Lezama, [d] M. Teresa González, [e] Edmund Leary, [e] Víctor Blanco, [a] Joel G. Fallaque, [ef] Cristina Díaz, [g] Fernando Martín, [efh] Juan M. Cuerva *[a] and Alba Millán *[a]

Received 13th June 2022,
Accepted 28th July 2022

DOI: 10.1039/d2tc02475f

rsc.li/materials-c

A direct, efficient and versatile strategy for the modulation of optoelectronic and magnetic properties of indeno[1,2-*b*]fluorene has been developed. 4-Substituted-2,6-dimethylphenyl acetylene groups placed in the apical carbon of the five-membered rings lead to redshifted absorption maxima (λ_{max} ranging from 600–700 nm) and considerable narrowing of the HOMO–LUMO energy gap (down to 1.5 eV). Experimental and theoretical data show an increase in the diradical character (y) and a decrease of the singlet-triplet energy gap. Moreover, we have investigated the single-molecule conductance of the antiaromatic indeno[1,2-*b*]fluorene for the first time by including thiomethyl (-SMe) anchor groups on the phenylacetylene moiety. Conductance values one order of magnitude higher than those of a reference linear 3-ring *para*-phenylene ethylene have been found, despite the longer length of the S-to-S molecular junction. First principles transport calculations support this high conductance value.

Introduction

Indeno[1,2-*b*]fluorene[1–6] (IF, **1**) is considered the formally antiaromatic analogue of pentacene. In contrast to the latter, IF displays high electron affinity due to the presence of the cyclopentadiene rings, thus narrowing the HOMO–LUMO energy gap.[1] This fact is explained by the existence of a central proaromatic *p*-quinodimethane (*p*-QDM) unit that presents a canonical diradical contribution (Fig. 1A).[6,7] The narrow HOMO–LUMO gap makes this molecule and their derivatives attractive for organic electronic devices[3,8–10] and complementary to acenes.[11] The challenge is to shield the highly reactive apical carbons at the five-membered ring (R group in Fig. 1A). In this sense, strategies to provide thermodynamic or kinetic stabilization are commonly used.[12,13] The most widely employed R groups are 2,4,6-trimethylphenyl (mesityl, Mes) and triisopropylsilyl (TIPS) acetylene. In addition to conferring stability,[14,15] these R groups have been proposed for the fine tuning of the optoelectronic properties of the systems although with a limited success. For example, Chase *et al.* demonstrated that the use of the electron-withdrawing TIPS acetylene produced a bathochromic shift in the UV-Vis absorption maxima in comparison to aryl groups such as Mes (Fig. 1B, **2** *vs.* **3**).[2,3] Modifications of the IF core would be in principle an alternative approach.[3] However, the incorporation of substituents at the 2- and 8-positions have almost no impact on the HOMO–LUMO gap tuning. For example, UV-Vis absorption maxima vary by 34 nm when different arenes are used as R groups (Fig. 1B, **3**) whilst the introduction of donor or acceptor groups (X) in the IF core only shifts the maxima 16 nm (Fig. 1B, **2**). The reason is related to a low HOMO/LUMO orbital density in those positions. To the best of our knowledge, the state of the art is represented by the work of Nishida *et al.* with the inclusion of α-substituted thienyl groups at the 6- and 12-positions (Fig. 1B, **3**),[4] the latter compound having the most red-shifted absorption maximum (607 nm) and the lowest HOMO–LUMO gap

[a] Departamento de Química Orgánica, Facultad de Ciencias, Unidad de Excelencia de Química Aplicada a Biomedicina y Medioambiente (UEQ), Universidad de Granada, 18071 Granada, Spain. E-mail: jmcuerva@ugr.es, amillan@ugr.es
[b] Departamento de Química Física Aplicada, Universidad Autónoma de Madrid, 28049 Madrid, Spain
[c] Centro de Instrumentación Científica, Universidad de Granada, 18071 Granada, Spain
[d] Departamento de Química Orgánica e Inorgánica, Facultad de Ciencia y Tecnología, Universidad del País Vasco, 48940, Leioa, Spain
[e] Fundación IMDEA Nanociencia, 28049, Madrid, Spain
[f] Departamento de Química, Módulo 13, Universidad Autónoma de Madrid, 28049, Madrid, Spain
[g] Departamento de Química Física, Facultad de Ciencias Químicas, Universidad Complutense de Madrid, 28040, Madrid, Spain
[h] Condensed Matter Physics Center (IFIMAC), 28049, Madrid, Spain

† Electronic supplementary information (ESI) available: Synthetic procedures and characterisation of new compounds, NMR spectra, high-resolution mass spectra, single-crystal X-Ray diffraction details, UV-Vis spectra, voltammograms, electron spin resonance spectrum, computational details, STM-BJ experiments and analysis and cartesian coordinates. CCDC 2177496. For ESI and crystallographic data in CIF or other electronic format see DOI: https://doi.org/10.1039/d2tc02475f

‡ Dedicated to Professor Joan Bosch on occasion of his retirement.

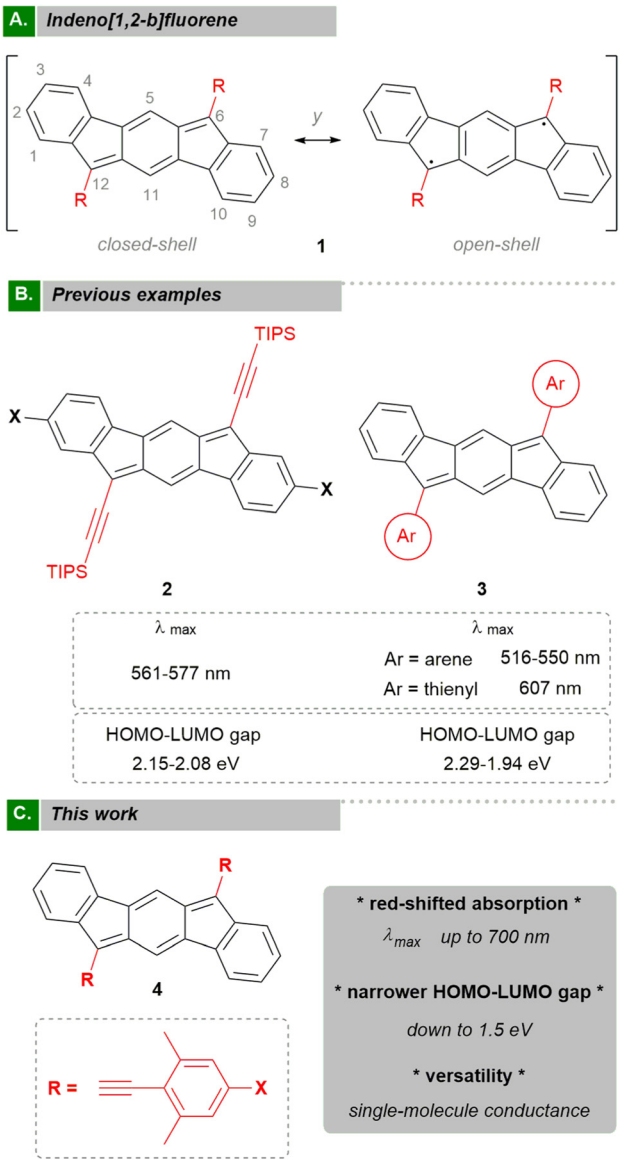

Fig. 1 (A) Resonance structures of indeno[1,2-*b*]fluorene; *y*: diradical character index (0 (closed-shell) ≤ *y* ≤ 1 (open-shell)). (B) Previous examples of indeno[1,2-*b*]fluorenes; X = donor/acceptor groups; Ar = arene or thienyl; HOMO–LUMO energy gap values estimated from optical properties. (C) Our approach to modulate optoelectronic properties of indeno[1,2-*b*]fluorene; X = donor/acceptor groups.

(1.94 eV) to date. Thus, a new approach to achieve a substantial modification of energy gap values in a predictable way is most desirable.

This HOMO–LUMO gap engineering would be useful to modulate the optical properties and also the electron transport through the molecule even at the single-molecule level. In this latter context, the energy gap narrowing offers the possibility of bringing the HOMO/LUMO levels closer to the Fermi level of the metal, in order to achieve high conductance potentially *via* a resonant transport mechanism. In a simple view of electron transport this is an optimal situation and it has been proposed as the origin of the greater conductance of antiaromatic systems over aromatic ones.[16–18] Nevertheless, the electron transport through antiaromatic hydrocarbons at the single-molecule level is still understudied, and experimental results do not always follow this expectation. For example, the 12π-electron antiaromatic biphenylene core was thoroughly investigated by Gantenbein *et al.*[19] They observed slight differences between conductance (G) values for biphenylene and its non-antiaromatic counterpart, fluorene ($\log(G/G_0)$ =–4.9 *vs.*–4.8, where $G_0 = 2e^2/h$). These results agreed with those reported previously by Schneebeli *et al.*[20] and show that for the smallest systems any differences due to antiaromaticity do not appear in the measured conductance.[16] Clearer results were observed by Schmidt *et al.* for the 16π-electron dibenzo[*a*,*e*]pentalene (DBP). They measured the conductance through the pentalene central core and compared it with an aromatic anthracene analogue. Here, a small increase was found between the anthracene and antiaromatic DBP ($\log(G/G_0) = -4.4$ *vs.* -4.3, respectively).[21] Fujii *et al.* found that an antiaromatic norcorrole nickel complex was about one order of magnitude more conductive than an aromatic nickel-porphyrin analogue.[18] The norcorrole compound is, however, slightly smaller than the porphyrin, so at least some of the conductance gain could be accounted for from the length change. Apart from these examples, there are no other conductance measurements on antiaromatic polycyclic hydrocarbons,[22,23] mainly due to the demanding synthesis and inherent instability.

Here, we present a set of novel indeno[1,2-*b*]fluorenes (20π-electrons), the next in the Hückel's 4n π-electron counting series, in which the HOMO–LUMO gap is tuned from ∼1.8 eV down to 1.5 eV resulting in an absorption maxima displacement of up to ∼100 nm with respect to the indeno[1,2-*b*]fluorene described by Nishida *et al.*[4] Our approach is based on a stabilizing group consisting of 2,4,6-substituted phenyl acetylenes, which permits the fine-tuning of the optoelectronic and magnetic properties of indeno[1,2-*b*]fluorene (Fig. 1C). It is worth noting that the common core can be electronically coupled with different donor and acceptor groups in the 4-position of the phenyl acetylene moiety, which can be subsequently used for different purposes. In particular, the inclusion of anchoring groups for gold electrodes (SMe) allows us to measure the single-molecule conductance of indeno[1,2-*b*]fluorene for the first time, observing an unusually high conductivity in comparison with that of the dibenzopentalene analogue owing to the HOMO–LUMO gap narrowing. All these results have been rationalized using quantum chemical calculations.

Results and discussion

Firstly, we synthesized the known diketone **5**[24] that provides the common IF core. Then different alkynes **6a–h** were prepared following a general strategy based on the Sonogashira cross-coupling reaction[25] using trimethylsilylacetylene and the corresponding iodoarenes, and finally deprotection of the alkyne-protecting group (see ESI,† for details). With both

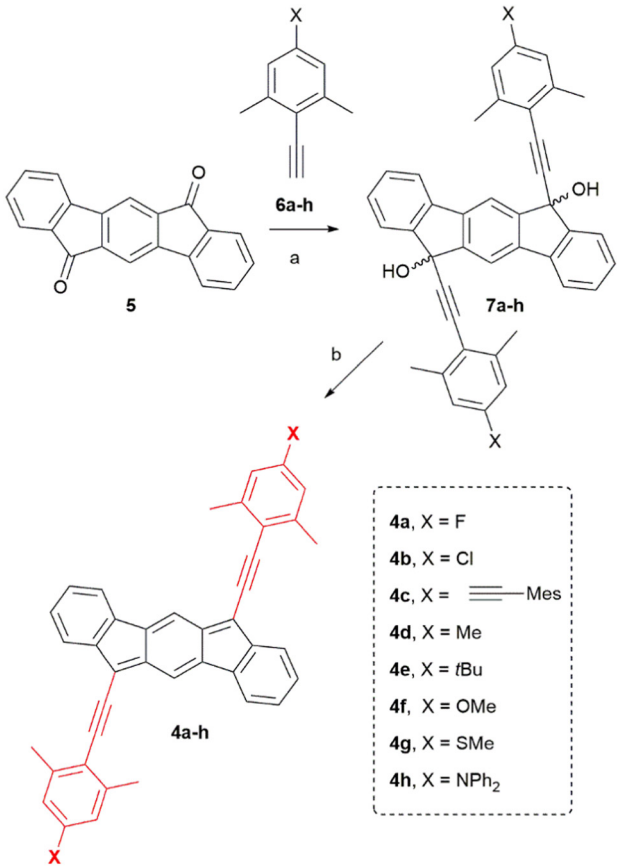

Scheme 1 Synthesis of compounds **4a–h**. (a) *n*-BuLi, THF, 0 °C to rt, 3 h; (b) $SnCl_2$, toluene, 40 °C, 15 min.

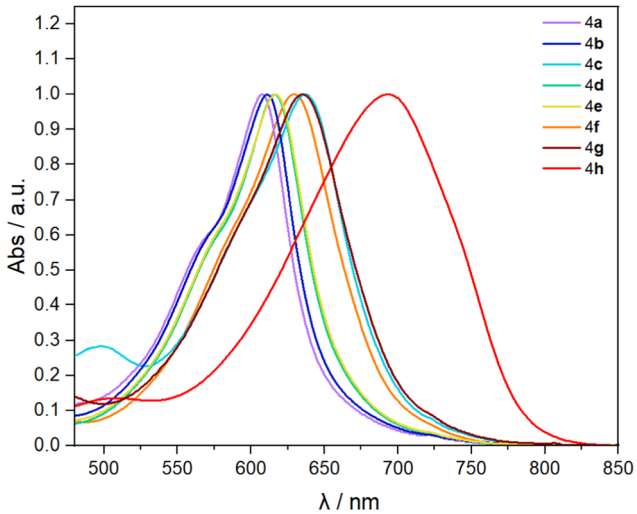

Fig. 2 Normalized electronic absorption spectra for compounds **4a–h**. All spectra were recorded in CH_2Cl_2 at 25 μM.

building blocks in our hands, we prepared a variety of indeno[1,2-*b*]fluorenes (**4a–h**) bearing both electron withdrawing and electron donating groups at the 4-position of the arene (X group in Scheme 1). For that, we carried out nucleophilic addition of the corresponding lithiated alkynes **6a–h** to diketone **5** to give diols **7a–h**. Subsequent dearomatization using $SnCl_2$ gave the final products **4a–h** as deep blue air-stable solids.

In general, compounds **4a–h** are highly insoluble in a wide range of organic solvents at typical NMR concentrations, which precludes characterization by ^{13}C-NMR in most of the cases. Nevertheless, the exact mass and isotopic distribution pattern of the peak corresponding to the $[M]^+$ species in the high-resolution mass spectra were in good agreement with the theoretical data in all cases. It is worth mentioning that blocking the *ortho*- and *para*-position of the arene is key in order to ensure air stability. On the one hand, dearomatization reactions on products bearing either 4-*t*Bu-phenylacetylene or 4-SMe-phenylacetylene fragments at the 6- and 12-positions gave messy reaction crudes. On the other hand, IF bearing 2,6-dimethylphenylacetylene decomposed in minutes. Increased stability by blocking *ortho*- and *para*-positions in the arene has been inspected from a theoretical point of view, through the spin density distribution (see Section S9.6 in the ESI†). In addition, **4d** and **4e** were checked by UV-Vis after several days not observing any significant change in their UV-Vis absorption profiles (see ESI,† Section S6.1).

Then we investigate the optoelectronic properties. Fig. 2 shows the UV-Vis absorption spectra of each compound recorded in CH_2Cl_2 solution.[26] In general, the phenylacetylene group in the 6,12-IF position induces a larger bathochromic shift in absorption maxima compared to **2** and **3** (Fig. 1B and Table 1). We can see low-energy absorption maxima spanning almost 100 nm from λ_{max} = 608 nm for the electron-withdrawing fluorine substituent (**4a**) to λ_{max} = 694 nm for the electron-donating diphenylamine group (**4h**). Remarkably, these data are comparable to those reported for much more extended indeno[1,2-*b*]fluorene cores.[27–29]

Vertical excitation energies were calculated by means of the TD-DFT approach, predicting absorption spectra (Fig. S27 and Table S4, ESI†), with energies within 0.3 eV of the measured values. The lowest-lying energy electronic transition corresponds to a HOMO → LUMO excitation, which redshifts with the strength of the electron-donating substituent in the 4-position (X group) of the phenyl group, according to the predicted narrowing of the HOMO–LUMO gap (see Table 1 and Table S2 in the ESI†); and in full agreement with the experimental trend observed for the absorption maxima and the optical gap. A full description of the employed computational methods is presented in the ESI.†

In general, our optical energy gap values are considerably lower (1.55–1.84 eV) than those reported before for indeno[1,2-*b*]fluorenes (1.9–2.2 eV).[1–6] We highlight the case of **4h**, for which we estimated an optical gap of 1.55 eV, the lowest reported to date for non-extended indeno[1,2-*b*]fluorene. As for other IF derivatives, compounds **4a–h** are all non-emissive.[30]

Cyclic voltamograms (CVs) for compounds **4a** and **4h** are shown in Fig. 3 (see ESI,† Section S7 for CVs of the other compounds). Data are depicted in Table 1, which shows the half-potentials ($E_{ox/red}$) of the reversible waves or the potential

Table 1 Optical, electrochemical and computational data of reported compounds **2a** (X = H) and **3a** (Ar = Mes) and compounds **4a–4h**

	Optical data[a]		Electrochemical data[b]					Computational data[c]		
Comp.	λ_{max}	E_{gap}	E_{ox}/E_{pa}	E_{red}/E_{pc}	E_{HOMO}	E_{LUMO}	E_{gap}	E_{HOMO}	E_{LUMO}	E_{gap}
2a[d]	568	2.12	1.20	−0.69, −1.20	−5.88	−4.00	1.88	−5.51	−3.47	2.04
3a[d]	516	2.29	1.10, 1.59	−1.12, −1.73	−5.78	−3.56	2.22	−5.34	−2.92	2.42
4a	608	1.84	0.61	−1.11, −1.47	−5.41	−3.69	1.72	−5.17	−3.47	1.71
4b	611	1.80	0.61	−1.07, −1.36	−5.41	−3.73	1.68	−5.23	−3.53	1.70
4c	637	1.72	—	−0.80, −1.00	n.d.	−4.00	n.d.	−4.99	−3.42	1.57
4d	616	1.78	0.59	−1.33	−5.39	−3.47	1.92	−4.98	−3.29	1.69
4e	616	1.79	0.62	−1.24	−5.42	−3.56	1.86	−4.98	−3.28	1.69
4f	630	1.73	0.66	−1.13	−5.46	−3.67	1.79	−4.83	−3.18	1.65
4g	636	1.70	0.41	−1.14	−5.21	−3.66	1.55	−4.90	−3.28	1.62
4h	694	1.55	0.23, 0.64	−1.11, −1.55	−5.03	−3.69	1.34	−4.71	−3.17	1.54

[a] Spectra were obtained in CH_2Cl_2; wavelengths are in nm. The optical HOMO–LUMO gap was determined as the intersection of the *x* axis and a tangent line passing through the inflection point of the lowest-energy absorption; energies are in eV. [b] CVs were recorded using 1.5 mM of compound in 0.1 M of Bu_4NPF_6 in CH_2Cl_2 at a scan rate of 50 mV s^{-1}. A glassy carbon disc was used as the working electrode, a Pt wire as the counter electrode, and a Ag wire as the pseudo-reference electrode. $E_{ox/red}$ is the half-wave potential ($E_{1/2}$) for reversible/quasi-reversible processes or the potential of the peak anodic (E_{pa}) or cathodic current (E_{pc}) for irreversible processes. Potential values are reported in V *vs.* Fc^+/Fc. HOMO and LUMO energies were estimated from first oxidation/reduction peak assuming an ionization energy of 4.8 eV for ferrocene. [c] Calculations performed at the the B3LYP/6-311+G** level of theory; energies in eV. [d] Data taken from ref. 3.

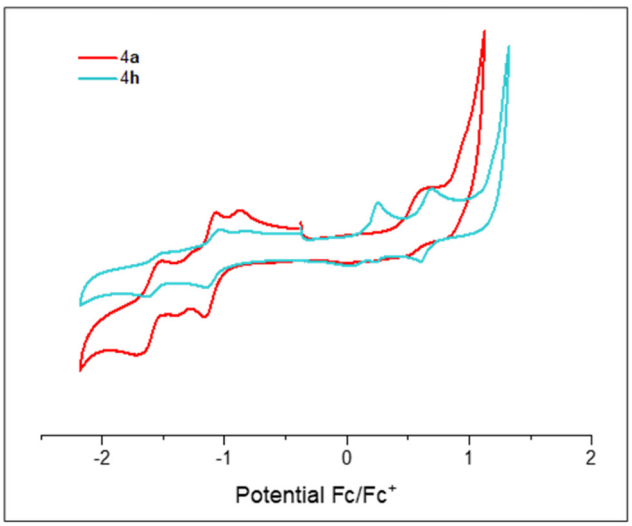

Fig. 3 Cyclic voltammograms (CVs) for **4a** and **4h**.

of peak current ($E_{pa/pc}$) for irreversible ones. We observed that every compound (**4a-h**) can accept at least one electron. In addition, **4a–4c** and **4h** show a second reduction event. In general, the potential values of the first cathodic peaks at approximately −0.8 to −1.33 V are in agreement with other related compounds.[2–4] In principle, more electron-withdrawing groups should stabilize anionic species, giving less negative values. However, this trend is not observed in our compounds **4a–h** as can be seen in the representative examples shown in Fig. 3. Both compound **4a** and **4h** display a first reversible wave at E_{red}= −1.11 V, making the presence of either acceptor or donor group inconsequential (**4a** (F) and **4h** (NPh_2) respectively). This is consistent with the distribution of the LUMO orbital over the system, which is mainly located on the central core (see ESI,† Section S9.3). Remarkably, compounds **4a**, **4b** and **4d–4h** gave an oxidation peak at a low-voltage potential (from +0.23 to +0.66 V) that translates as a raising of the HOMO energy. These observations can be explained by an increase in overall electron-density on the systems provided by the phenylacetylene moiety.

Consequently, the estimated electrochemical HOMO–LUMO gaps are reduced considerably in comparison to other indeno[1,2-*b*]fluorenes.[1–6] Interestingly, the electrochemically determined energy gaps are lower than optical and computational values which have been also observed for other examples of indeno[1,2-*b*]fluorenes.[2–4] In any case, the trend is quite consistent for all three data sets.

As explained in the introduction (Fig. 1A), the resonance between the closed-shell and the open-shell forms implies that indeno[1,2-*b*]fluorene could be a potential diradical. Diradicals have been postulated as building blocks for magnetically active materials.[31–33] For that, a transition between the singlet and the triplet state (low- to high-spin) should occur and its energy should be low in order to facilitate the switching processes. As the HOMO–LUMO gap is supposed to trend with singlet–triplet energy gaps[34] (ΔE_{ST}, the energy difference between the singlet ground electronic state and the lowest-lying triplet excited state), we wondered whether our phenylacetylene groups could serve to tune this key parameter. We select **4d** as a model compound due to its structural resemblance to other reported indeno[1,2-*b*]fluorenes (*e.g.* **2a** and **3a**).[2,3] We analysed compound **4d** by electron paramagnetic resonance (EPR) spectroscopy. Interestingly, **4d** is not silent, indicating the presence of paramagnetic species. We observed a very weak signal for **4d** at room temperature which could correspond to a small population of the triplet species (see ESI,† Section S8). This phenomenon has not been observed in other indeno[1,2-*b*]fluorenes before.[35] To gain insight into this result, first, the open-shell singlet character for **2a** (X = H), **3a** (Ar = Mes) and **4d** were evaluated with DFT using the diradical character index (*y*). A negligible *y* value was calculated for **3a** (0.090); meanwhile a similar value of 0.30 and 0.36 has been estimated for **2a** and **4d**, respectively. DFT calculations of ΔE_{ST} for **2a**, **3a** and **4d**[36] estimate a decrease in the singlet-triplet energy gaps of over

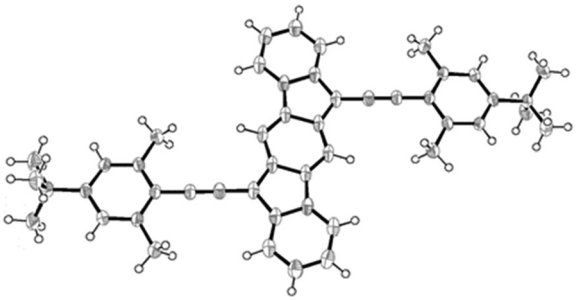

Fig. 4 ORTEP drawing of the X-ray crystal structure of compound **4e**, showing the thermal ellipsoids at 50% probability.

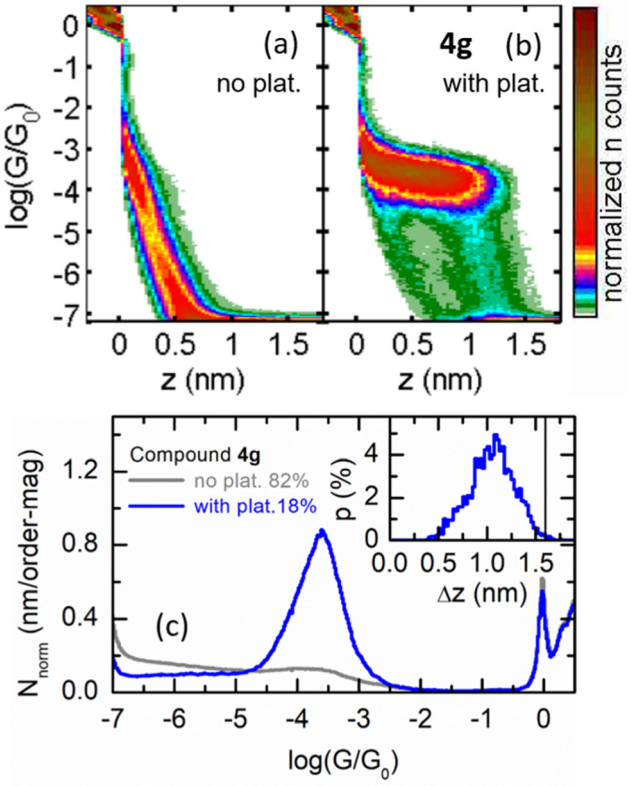

Fig. 5 (a) and (b) 2D histograms for compound **4g** built from traces without (a) and with (b) plateaus. (c) Corresponding 1D histograms. The inset in (c) shows the plateau-length distribution for the traces with plateaus, where the black vertical line corresponds to the expected plateau length for a S-to-S molecular bridge with the molecule fully stretched between the apexes of the electrodes. For details of sample preparation and methodology, see ESI,† Section S10.

7 kcal mol^{-1} compared to other reported indeno[1,2-*b*]fluorene structures (10.7 kcal mol^{-1} for **4d** *vs.* 18.24 kcal mol^{-1} for **3a**) (see ESI,† Sections S9.4 and S9.5).

This greater diradical character should reflect in the C–C bond distances of the central *p*-QDM unit. To evaluate this, we attempted the crystallization of compound **4d**. However, this compound was challenging to crystallize, and no suitable crystals were obtained in a variety of solvent mixtures and/or applying different crystallization techniques. Fortunately, we did obtain single crystals of **4e** (bearing a *t*Bu instead of Me) and this compound was characterized by X-ray diffraction (Fig. 4).[37] The compound **4e** has helped to complete the study since it shows the same electronic and diradical properties as **4d**, (see ESI,† for comparison, Sections S9.1 and S9.5). The structure of **4e** was confirmed and bond lengths were analysed.

The molecule features the distinct *p*-QDM unit within the core, with alternating long (1.418 Å and 1.451 Å) and short (1.397 Å and 1.361 Å) C–C bond lengths. However, **4e** contains longer double bonds and shorter single bonds in comparison to previously reported ones (see ESI,† Table S1).[2–4] promoting a slight gain in aromatic character for the central *p*-QDM unit. Quantum chemical DFT calculations reproduce the observed lengthening/shortening of double/single bonds, (see Table S3 in ESI†) testing the structural similarity with **4d**. In addition, calculated nucleus independent chemical shift (NICS) indices for the open-shell singlet state are consistent with an increase in the aromaticity of the central benzenoid ring of **4e** (and therefore **4d**) in comparison to **3a** (see ESI,† Fig. S40), supporting also the higher diradical character and smaller singlet–triplet energy gap presented above. All these results suggest that **4e** has a modest open-shell (diradical) singlet system in the ground state. Although the triplet state is only partially accessible at room temperature and these structures are better described as closed-shell molecules, these results open a promising approach to tune ΔE_{ST} in a straightforward manner, just by changing the stabilizing group.

Finally, to show the versatility of this stabilizing group, we focus on compound **4g**. The introduction of the thiomethyl group (-SMe) makes this molecule suitable for single-molecule conductance measurements by means of the scanning tunneling microscopy break-junction technique (STM-BJ).[38] These experiments are based on a push–pull process between the STM gold tip and the substrate. During the pulling, G decreases with the distance between electrodes (z), displaying regions of constant conductance (plateaus) at $G < G_0$ if molecular junctions are formed between the metallic electrodes. SMe anchor groups have been widely used in conductance studies[39,40] and avoid known drawbacks related to the use of thiol groups and gold electrodes.[41] In addition, the introduction of the alkyne spacer offers a double advantage: (i) to avoid a permanent torsion of the phenyl group which would hamper electron transport,[42,43] and (ii) to promote a narrowing of the HOMO–LUMO gap as has been formerly proved. Fig. 5 displays 2D G *vs.* z and 1D G histograms obtained for **4g**. We found that 18% of the pulling G *vs.* z traces showed plateaus (total number of traces ~11 800), which produced a well-defined cloud in their 2D histogram (Fig. 5b) in contrast with the smooth exponential decay of the traces without plateaus (Fig. 5a). This cloud translates into a quasi-symmetric Gaussian type curve in the 1D G histogram (Fig. 5c) with a peak centered at log (G/G_0) = −3.6, with a half width at half maximum (HWHM) of 0.36. Fig. 5c (inset) shows that the plateau-length distribution peaks at 1.1 nm (HWHM = 0.5 nm), while it reaches its maximum values at the expected Au-to-Au molecular bridge length, once the typical gold retraction after breakage is subtracted

(2.1 nm minus 0.4 nm), indicated by a vertical black line in the figure. These plateau-length distribution features are typical for SMe-terminated compounds, with molecules fully extended between the gold electrodes for the longest conductance plateaus.

It is remarkable that the conductance value observed for **4g** is one order of magnitude higher than that of the slightly shorter 3-ring reference *p*-phenylene ethylene (**OPE3-SMe**).[44] In addition, the conductance of **4g** is more than half order of magnitude greater than that observed for a similar dibenzopentalene (DBP) compound, also with SMe anchor groups ($\log(G/G_0) = -4.3$) which has two fewer bonds along the shortest S-to-S pathway.[21] This behaviour is noteworthy because the relationship between the degree of aromaticity/antiaromaticity and molecular conductance in neutral molecules is under debate and there is no clear consensus in the literature. For example, Chen *et al.* concluded that for a family of amine-terminated wires containing either thiophene, oxazole or cyclopentadiene, the conductance was lowest for the thiophene derivative, which is formally the most aromatic of the three.[16] On the other hand, Yang *et al.* studied a similar family of 2,5-disubstituted 5-membered heterocycles, this time with pyridyl anchor groups. Here, however, they did not find any correlation between conductance and aromaticity.[23a]

It is insightful to compare the properties of compound **4g** with the **DBP-SMe** previously studied.[21] The electrochemical HOMO–LUMO gaps of the two are 1.55 eV and 1.99 eV respectively. Our NICS calculations show that the central 5–6–5 rings are quite strongly antiaromatic which is reflected in the low electrochemical HOMO–LUMO gap of 1.55 eV. The gap is about 20% narrower than for the dibenzopentalene previously studied which suggests **4g** has greater antiaromatic character. Our results thus demonstrate that despite the slight length increase of **4g** over **DBP-SMe**, the reduced HOMO–LUMO gap as a consequence of the greater antiaromatic character is more than enough to outweigh this difference.

Fig. S41 (ESI†) compares conductance *vs* voltage (*G*–*V*) curves for both compounds, recorded by sweeping the voltage between −1 V and +1 V at different positions along the conductance plateaus.[45] The increase in conductance above ±0.6 V observed for **4g** is in contrast with flatter *G*–*V* curves of dibenzopentalene,[21] and points towards the closest molecular level of **4g** being closer in energy to the gold Fermi level than that of dibenzopentalene, in agreement with the greater observed low-bias conductance.

Overall, this comparison suggests that the reason for the higher conductance of **4g** over **DBP-SMe** is its smaller HOMO–LUMO gap, which is a direct consequence of its enhanced antiaromatic character. Perhaps this is not quite the reasoning suggested by Breslow as to why conductance should correlate with the degree of aromatic/antiaromatic character, but it suggests that the general intuition is nonetheless correct.

In order to rationalize this experimental result, first principles calculations were carried out to compute the zero-bias DFT+Σ transmission function within the Landauer formalism. The end-to-end molecule arrangement within the junction was considered. All the details are described in Section S9.7 of the ESI.† From the single-molecule junction optimized geometry, an S-to-S vertical distance of 2.12 nm is obtained, in full agreement with the value estimated experimentally. In addition, a conductance value of $\log(G/G_0) = -3.27$ is calculated as the logarithm of the transmission probability at the Fermi level, in reasonable agreement with the experimental value.

The structure of compound **4g** in the junction has been evaluated through the NICS index, and compared with that of molecule **4d (4e)**. As is shown in Fig. S40 and Table S6 in the ESI,† molecule **4g** shows the same aromatic/antiaromatic character profile than compound **4d (4e)** in the singlet state: aromatic external six-member rings, anti-aromatic five-member rings and less/more aromatic central *p*-QMD unit than the six/five rings. Quantitatively, external, and central six-member rings are slightly less aromatic than in the **4d (4e)** case, indicating the closed-shell nature of this system into the junction.

Conclusions

In conclusion, a new strategy for narrowing the HOMO–LUMO energy gap of indeno[1,2-*b*]fluorene has been developed. The approach is based on the inclusion of different 4-substituted-2,6-dimethylphenyl acetylenes at the five-membered ring apical carbon atoms. This substitution maintains the stability while shifting absorption maxima to the 600–700 nm region corresponding to a narrower HOMO–LUMO gap. Thus, in comparison to other reported indeno[1,2-*b*]fluorene, a considerable overall decrease (down to ∼1.8–1.5 eV) is achieved. Interestingly, this approach also allowed us to tune the diradical character and the singlet-triplet energy gap and could be an appealing strategy to apply to other potential diradical structures. This is something we will be pursuing in future studies. In addition, we report single-molecule conductance measurements for the antiaromatic indeno[1,2-*b*]fluorene for the first time thanks to the introduction of anchoring groups (-SMe) in the phenylacetylene fragment. Our results show an unusually high conductance value for such a long molecule. This remarkable example adds to the very few studies of single-molecule conductance on antiaromatic molecular bridges and reinforces the idea that the smaller the energy gap, the larger the conductance value due to a better alignment of the HOMO/LUMO molecular orbitals with respect to the Fermi level of the metal. Our experimental results fit remarkably well with the theoretical calculations.

Author contributions

Conceptualization: J. M. C., A. M.; data curation: S. R. G., J. G. F., C. D., F. M.; formal analysis: R. C., A. M P., S. R. G., I. R. M., L. L., M. T. G., E. L., V. B., J. M. C., A. M.; funding acquisition: F. M. J. M. C., A. M.; investigation: R. C., A. M. P., I. R. M.; methodology: R. C., A. M. P.; project administration: J. M. C., A. M.; resources: J. M. C., A. M., F. M.; software: S. R. G., M. T. G., E. L., J. G. F., C. D., F. M.; supervision: J. M. C., A. M.; validation: R. C., A. M. P.; visualization: R. C., S. R. G., M. T. G.,

A. M.; writing – original draft: J. M. C., A. M.; writing – review & editing: all authors.

Conflicts of interest

There are no conflicts to declare.

Acknowledgements

We acknowledge funding from MCIN/AEI/10.13039/5011000-11033 and ''ERDF A way of making Europe'' (PGC2018-101873-A-I00), FEDER/Junta de Andalucía-Consejería de Economía y Conocimiento (A-FQM-221-UGR18), and the Ministerio de Ciencia e Innovación (PID2019-106732GB-I00, PID2019-105458RB-I00), 'Severo Ochoa' Programme for Centers of Excellence in R&D SEV-2016-0686, and 'María de Maeztu' Programme for Units of Excellence in R&D CEX2018- 000805-M). R. C. thanks the Ministerio de Ciencia e Innovación for a FPI contract (PRE2018-083406). A. M.-P. thanks the Ministerio de Universidades for a FPU contract (FPU19/03751). I. R. M. thanks MCIN/AEI/10.13039/501100011033 for a Personal Técnico de Apoyo contract (PTA2017-13681-I). E. L. thanks the Comunidad de Madrid Atracción de Talento grant 2019-T1/IND-16384. J. G. F. thanks the FPI program of the MCIN co-financed by the European Social Found. We acknowledge the allocation of computer time by the Red Española de Supercomputación and the Centro de Computación Científica at Universidad Autónoma de Madrid (CCC-UAM).

References

1 D. T. Chase, B. D. Rose, S. P. McClintock, L. N. Zakharov and M. M. Haley, *Angew. Chem., Int. Ed.*, 2011, **50**, 1127.
2 D. T. Chase, A. G. Fix, B. D. Rose, C. D. Weber, S. Nobusue, C. E. Stockwell, L. N. Zakharov, M. C. Lonergan and M. M. Haley, *Angew. Chem., Int. Ed.*, 2011, **50**, 11103.
3 D. T. Chase, A. G. Fix, S. J. Kang, B. D. Rose, C. D. Weber, Y. Zhong, L. N. Zakharov, M. C. Lonergan, C. Nuckolls and M. M. Haley, *J. Am. Chem. Soc.*, 2012, **134**, 10349.
4 J.-i Nishida, S. Tsukaguchi and Y. Yamashita, *Chem. – Eur. J.*, 2012, **18**, 8964.
5 B. D. Rose, N. J. Sumner, A. S. Filatov, S. J. Peters, L. N. Zakharov, M. A. Petrukhina and M. M. Haley, *J. Am. Chem. Soc.*, 2014, **136**, 9181.
6 C. K. Frederickson, B. D. Rose and M. M. Haley, *Acc. Chem. Res.*, 2017, **50**, 977.
7 M. Abe, *Chem. Rev.*, 2013, **113**, 7011.
8 I. Martínez, X. Zarate, E. Schott, C. Morales-Verdejo, F. Castillo, J. M. Manríquez and I. Chávez, *Chem. Phys. Lett.*, 2015, **636**, 31.
9 A. M. Zeidell, L. Jennings, C. K. Frederickson, Q. Ai, J. J. Dressler, L. N. Zakharov, C. Risko, M. M. Haley and O. D. Jurchescu, *Chem. Mater.*, 2019, **31**, 6962.
10 A. Can, A. Facchetti and H. Usta, *J. Mater. Chem. C*, 2022, **10**, 8496.
11 J. E. Anthony, *Angew. Chem., Int. Ed.*, 2008, **47**, 452.
12 K. Kato and A. Osuka, *Angew. Chem., Int. Ed.*, 2019, **58**, 8978.
13 B. Tang, J. Zhao, J.-F. Xu and X. Zhang, *Chem. Sci.*, 2020, **11**, 1192.
14 The less hindered trimethylsilylacetylene R group gives di-, tri- and oligomerization of [1,2-*b*]IF. See: X. Fu and D. Zhao, *Org. Lett.*, 2015, **17**, 5694.
15 The bare [1,2-*b*]-IF structure has been generated on-surface. See: Z. Majzik, N. Pavliček, M. Vilas-Varela, D. Pérez, N. Moll, E. Guitián, G. Meyer, D. Peña and L. Gross, *Nat. Commun.*, 2018, **9**, 1198.
16 W. Chen, H. Li, J. R. Widawsky, C. Appayee, L. Venkataraman and R. Breslow, *J. Am. Chem. Soc.*, 2014, **136**, 918.
17 R. Breslow and F. W. Foss, *J. Phys.: Condens. Matter*, 2008, **20**, 374104.
18 S. Fujii, S. Marqués-González, J.-Y. Shin, H. Shinokubo, T. Masuda, T. Nishino, N. P. Arasu, H. Vázquez and M. Kiguchi, *Nat. Commun.*, 2017, **8**, 15984.
19 M. Gantenbein, X. Li, S. Sangtarash, J. Bai, G. Olsen, A. Alqorashi, W. Hong, C. J. Lambert and M. R. Bryce, *Nanoscale*, 2019, **11**, 20659.
20 S. Schneebeli, M. Kamenetska, F. Foss, H. Vazquez, R. Skouta, M. Hybertsen, L. Venkataraman and R. Breslow, *Org. Lett.*, 2010, **12**, 4114.
21 M. Schmidt, D. Wassy, M. Hermann, M. T. González, N. Agraït, L. A. Zotti, B. Esser and E. Leary, *Chem. Commun.*, 2021, **57**, 745.
22 For other experimental studies based on antiaromatic molecules see ref. 18 and: X. Yin, Y. Zang, L. Zhu, J. Z. Low, Z.-F. Liu, J. Cui, J. B. Neaton, L. Venkataraman and L. M. Campos, *Sci. Adv.*, 2017, **3**, eaao2615.
23 For experimental studies concerning aromaticity-conductance relationship: (*a*) Y. Yang, M. Gantenbein, A. Alqorashi, J. Wei, S. Sangtarash, D. Hu, H. Sadeghi, R. Zhang, J. Pi, L. Chen, X. Huang, R. Li, J. Liu, J. Shi, W. Hong, C. J. Lambert and M. R. Bryce, *J. Phys. Chem. C*, 2018, **122**, 14965; (*b*) M. Gantenbein, L. Wang, A. A. Al-jobory, A. K. Ismael, C. J. Lambert, W. Hong and M. R. Bryce, *Sci. Rep.*, 2017, **7**, 1794; (*c*) A. Mahendran, P. Gopinath and R. Breslow, *Tetrahedron Lett.*, 2015, **56**, 4833.
24 S. Merlet, M. Birau and Z. Y. Wang, *Org. Lett.*, 2002, **13**, 2157.
25 R. Chinchilla and C. Najera, *Chem. Rev.*, 2007, **107**, 874.
26 Individual UV-Vis spectra are provided in the ESI,† Section S6.
27 C. K. Frederickson, L. N. Zakharov and M. M. Haley, *J. Am. Chem. Soc.*, 2016, **138**, 16827.
28 G. E. Rudebusch, J. L. Zafra, K. Jorner, K. Fukuda, J. L. Marshall, I. Arrechea-Marcos, G. L. Espejo, R. Ponce Ortiz, C. J. Gómez-García, L. N. Zakharov, M. Nakano, H. Ottosson, J. Casado and M. M. Haley, *Nat. Chem.*, 2016, **8**, 753.
29 C. K. Frederickson, J. E. Barker, J. J. Dressler, Z. Zhou, E. R. Hanks, J. P. Bard, L. N. Zakharov, M. A. Petrukhina and M. M. Haley, *Synlett*, 2018, 2562.
30 B. D. Rose, L. E. Shoer, M. R. Wasielewski and M. M. Haley, *Chem. Phys. Lett.*, 2014, **616-617**, 137.

31 A. Rajca, *Chem. Rev.*, 1994, **94**, 871.
32 X. Hu, W. Wang, D. Wang and Y. Zheng, *J. Mater. Chem. C*, 2018, **6**, 11232.
33 P. Murto and H. Bronstein, *J. Mater. Chem. C*, 2022, **10**, 7368.
34 (*a*) M. Nakano, *Top. Curr. Chem.*, 2017, **375**, 47; (*b*) A. S. Hacker, M. Pavano, J. E. Wood, H. Hashimoto, K. M. D'Ambrosio, C. K. Frederickson, J. L. Zafra, C. J. Gómez-García, V. Postils, A. R. McDonald, D. Casanova, D. K. Frantz and J. Casado, *Chem. Commun.*, 2019, **55**, 14186.
35 Although we cannot rule out the presence of a radical impurity, the detection of a signal in the $\Delta ms = \pm 2$ region suggests that the species should be a triplet. Thus, mono-radical impurity can be almost discarded. We submitted the sample to ICP-MS analysis before the EPR measurement to detect inorganic impurities. Different metals were detected but in ppm concentrations.
36 Usually, these calculations are carried out replacing the R groups for simpler groups such as methyl in order to reduce calculation time. In this case, we have calculated ΔE_{ST} for the whole structures.
37 Deposition number 2177496† contains the supplementary crystallographic data for this paper. ORTEP-3 software was used to create the ellipsoid picture: L. J. Farrugia, *J. Appl. Crystallogr.*, 2012, **45**, 849.
38 B. Xu and J. N. Tao, *Science*, 2003, **301**, 1221.
39 Y. S. Park, A. C. Whalley, M. Kamenetska, M. L. Steigerwald, M. S. Hybertsen, C. Nuckolls and L. Venkataraman, *J. Am. Chem. Soc.*, 2007, **129**, 15768.
40 M. Frei, S. V. Aradhya, M. S. Hybertsen and L. Venkataraman, *J. Am. Chem. Soc.*, 2012, **134**, 4003.
41 E. Leary, L. A. Zotti, D. Miguel, I. R. Márquez, L. Palomino-Ruiz, J. M. Cuerva, G. Rubio-Bollinger, M. T. González and N. Agraït, *J. Phys. Chem. C*, 2018, **122**, 3211.
42 L. Venkataraman, J. E. Klare, C. Nuckolls, M. S. Hybertsen and M. L. Steigerwald, *Nature*, 2006, **442**, 904.
43 A. Mishchenko, D. Vonlanthen, V. Meded, M. Bürkle, C. Li, I. V. Pobelov, A. Bagrets, J. K. Viljas, F. Pauly, F. Evers, M. Mayor and T. Wandlowski, *Nano Lett.*, 2010, **10**, 156.
44 D. Miguel, L. Álvarez de Cienfuegos, A. Martín-Lasanta, S. P. Morcillo, L. A. Zotti, E. Leary, M. Bürkle, Y. Asai, R. Jurado, D. J. Cárdenas, G. Rubio-Bollinger, N. Agraït, J. M. Cuerva and M. T. González, *J. Am. Chem. Soc.*, 2015, **137**, 13818.
45 *G–V* curves of the dibenzopentalene were reported in ref. 21 and replotted in the ESI† to compare with compound **4g**.